



OPEN

Multi-omics analysis of m⁶A modification-related patterns based on m⁶A regulators and tumor microenvironment infiltration in lung adenocarcinoma

Xincheng Wu¹ & Zhengping Bai²✉

Epigenetic modifications, especially N⁶-methyladenosine (m⁶A) modification, play a key role in tumor microenvironment (TME) infiltration. However, the regulatory role of m⁶A modification in the TME of lung adenocarcinoma (LUAD) remains unclear. A total of 2506 patients with LUAD were included in the analysis and divided into different groups according to distinct m⁶A modification-related patterns based on 23 m⁶A regulators. A comprehensive analysis was performed to explore TME infiltration in different m⁶A modification-related patterns. Principal component analysis was performed to obtain the m⁶Ascore and to quantify m⁶A modification-related patterns in different individuals. Three distinct m⁶A modification-related patterns were identified by 23 m⁶A regulators. The pathway enrichment analysis showed that m⁶Acluster-A was associated with immune activation; m⁶Acluster-B was associated with carcinogenic activation; m⁶Acluster-C was prominently related to substance metabolism. M⁶Acluster-A was remarkably rich in TME-infiltrating immune cells and patients with this pattern showed a survival advantage. The m⁶Ascore could predict TME infiltration, tumor mutation burden (TMB), the effect of tumor immunotherapy, and the prognosis of patients in LUAD. High m⁶Ascore was characterized by increased TME infiltration, reduced TMB, and survival advantage. Patients with a high m⁶Ascore exhibited significantly improved clinical response to anti-cytotoxic T lymphocyte antigen-4 (anti-CTLA4) immunotherapy. This study explored the regulatory mechanisms of TME infiltration in LUAD. The comprehensive analysis of m⁶A modification-related patterns may contribute to the development of individualized immunotherapy and the improvement of the overall effectiveness of immunotherapy for LUAD patients.

Lung cancer (LC), a fatal malignancy, has become a leading cause of malignant tumor-related death worldwide¹. The 5-year survival rate of LC at a localized stage, regional stage, and distant stage is 54%, 26%, and 4%, respectively². The prognosis of LC is poor, because approximately 57% of LC patients are diagnosed at the distant stage^{3,4}. LC can be histologically classified into non-small-cell lung cancer (NSCLC) and small-cell lung cancer (SCLC). NSCLC accounts for ~85% of all LC cases^{5,6}. Primary treatments for LUAD include surgery, chemotherapy, and radiotherapy. However, the prognosis of advanced LUAD remains poor due to limited treatment efficacy, which requires the development of new therapeutic targets and treatments.

Tumor growth and spread depend not only on tumor cell characteristics but also on the interaction between tumor cells and tumor microenvironment (TME), a cellular environment where tumors or cancer stem cells exist^{7–9}. TME consists of multiple components, including infiltrating immune cells¹⁰. TME plays a pivotal role in tumorigenesis, and its heterogeneity may lead to multiple dimensions in the therapeutic response and prognosis of patients^{11–14}. Immunotherapy using immune checkpoint inhibitors is based on TME cell infiltration and has become a promising treatment strategy for cancer patients, including LC¹⁵. The drugs that are widely used in LC immunotherapy include medications targeting programmed cell death protein 1 (PD-1) and cytotoxic T lymphocyte antigen-4 (CTLA4), such as Nivolumab and Ipilimumab⁷. Although a small proportion of cancer patients respond well to immunotherapy, the majority of them experience minimal or no clinical benefits¹⁶. In addition,

¹Hunan University of Chinese Medicine, 300 Xueshi Rd., Yuelu District 410208, Changsha, China. ²Hunan Academy of Chinese Medicine, 58 Lushan Rd., Yuelu District 410006, Changsha, China. ✉email: baizhengping@yeah.net

Regulator	Full name	Category	Regulator	Full name	Category
METTL3	Methyltransferase-like protein 3	Writer ¹	YTHDF3	YTH m ⁶ A RNA-binding protein 3	Reader
METTL14	Methyltransferase-like protein 14	Writer	HNRNPC	Heterogeneous nuclear ribonucleo-protein C	Reader
METTL16	Methyltransferase-like protein 16	Writer	FMR1	Fragile X mental retardation protein	Reader
WTAP	Wilms tumor 1-associated protein	Writer	LRPPRC	Leucine-rich PPR-motif-containing protein	Reader
VIRMA	Vir-like m ⁶ A methyltransferase associated protein	Writer	HNRNPA2B1	Heterogeneous nuclear ribonucleo-protein A2B1	Reader
ZC3H13	zinc finger CCCH domain-containing protein 13	Writer	IGFBP1	Insulin-like growth factor binding protein 1	Reader
RBM15	RNA-binding motif protein 15	Writer	IGFBP2	Insulin-like growth factor binding protein 2	Reader
RBM15B	RNA binding motif protein 15B	Writer	IGFBP3	Insulin-like growth factor binding protein 3	Reader
YTHDC1	YTH domain-containing 1	Reader ²	RBMX	X-linked RNA-binding motif protein	Reader
YTHDC2	YTH domain-containing 2	Reader	FTO	Fat mass and obesity-associated protein	Eraser ³
YTHDF1	YTH m ⁶ A RNA-binding protein 1	Reader	ALKBH5	Alk B homologue 5	Eraser
YTHDF2	YTH m ⁶ A RNA-binding protein 2	Reader			

Table 1. N⁶-methyladenosine (m⁶A) regulators. ¹The m⁶A methyltransferases catalyze the formation of m⁶A as m⁶A writers. ²The m⁶A demethylases remove the methyl codes from target RNAs as m⁶A erasers. ³The m⁶A-binding proteins recognize and bind to the m⁶A methylation sites in RNA as m⁶A readers.

the clinical application of immunotherapies is limited by their toxicity profiles^{17–19}. Future investigations on the diversity and complexity of TME may elucidate the effects of TME on tumor progression, immune escape, and immunotherapeutic response. Personalized immunotherapy may also be provided for LUAD patients based on the tumor-immune phenotypes identified by the analysis of TME heterogeneity.

N⁶-methyladenosine (m⁶A) modification, referring to methylation at the sixth N atom of adenine, is the third layer of epigenetic modification. It is the most common post-transcriptional modification on mRNA, long non-coding RNA, as well as microRNA^{20–24}. The m⁶A modification on RNA is a dynamic process involving binding proteins (“readers”), demethylases (“erasers”), and methyltransferases (“writers”), all of which are termed m⁶A regulators²⁵. The formation of m⁶A is catalyzed by methyltransferases. The binding proteins recognize and bind to m⁶A methylation sites, and the methyl codes of target RNAs are removed by demethylases^{26,27}. M⁶A modification is implicated in RNA transcription, processing, splicing, degradation, and translation^{28,29}. Aberrant m⁶A modification is closely associated with the onset and progression of tumors^{22,23}. The m⁶A regulators also play critical roles in tumorigenesis^{22,30,31}. Jin et al. found that ALKBH5 inhibited the expression of YAP via targeting the remover of m⁶A modification. In addition, YAP was negatively associated with the proliferation, invasion, migration, and epithelial-to-mesenchymal transition of NSCLC cells³². Taken together, m⁶A regulators-mediated m⁶A modification is implicated in the occurrence, progression, and prognosis of cancers, including LC.

Recent evidence has revealed that m⁶A modification is closely related to TME infiltration of immune cells, which affects immunotherapeutic responses³³. Wang et al. found that the suppression of m⁶A modification sensitized tumor cells to immunotherapy by altering TME and the recruitment of CD⁸⁺ tumor-infiltrating lymphocytes. In addition, the inhibition of m⁶A regulators improved the effectiveness of immunotherapies against colorectal cancer³⁴. Therefore, a comprehensive analysis of the correlation between TME and m⁶A regulators-mediated m⁶A modification may further elucidate the pathogenic mechanisms of LUAD and provide scientific support for the development of novel immunotherapy. In this study, the genomic data of LUAD samples were obtained from the public databases, and then used for comprehensive analyses of m⁶A modification-related patterns and the correlation between m⁶A regulators and TME infiltration. Three distinct m⁶A modification-related patterns with distinct degrees of TME cell infiltration were identified, suggesting that m⁶A modification played an indispensable role in the formation of TME. Moreover, a scoring system was developed to quantify m⁶A modification-related patterns in different individuals. This study may provide insights into a better understanding of TME-related regulatory mechanisms in LUAD and the optimization of personalized immunotherapy for LUAD patients.

Results

Genetic variation of m⁶A regulators in LUAD. A total of 23 m⁶A regulators, including 13 “readers”, 8 “writers”, and 2 “erasers”, were identified (Table 1). The incidence of CNV and somatic mutations of 23 m⁶A regulators in LUAD was summarized. The mutation of m⁶A regulators was observed in 115 out of 561 samples, with a frequency of 20.5%. ZC3H13 exhibited the highest mutation frequency among all m⁶A regulators (Fig. 1a). The CNV analysis was performed to show the CNV frequency of 23 regulators. Among them, YTHDF1, VIRMA, FMR1, METTL3, HNRNPC, RBMX, YTHDF3, HNRNPA2B1, LRPPRC, IGFBP1, IGFBP3, FTO, and YTHDC1 showed a trend of amplification, while YTHDF2, WTAP, YTHDC2, ALKBH5, IGFBP2, ZC3H13, RBM15, METTL14, RBM15B, and METTL16 had a high frequency of deletion (Fig. 1b). We then measured the mRNA levels of these regulators in LUAD and normal lung tissues. Compared with normal tis-

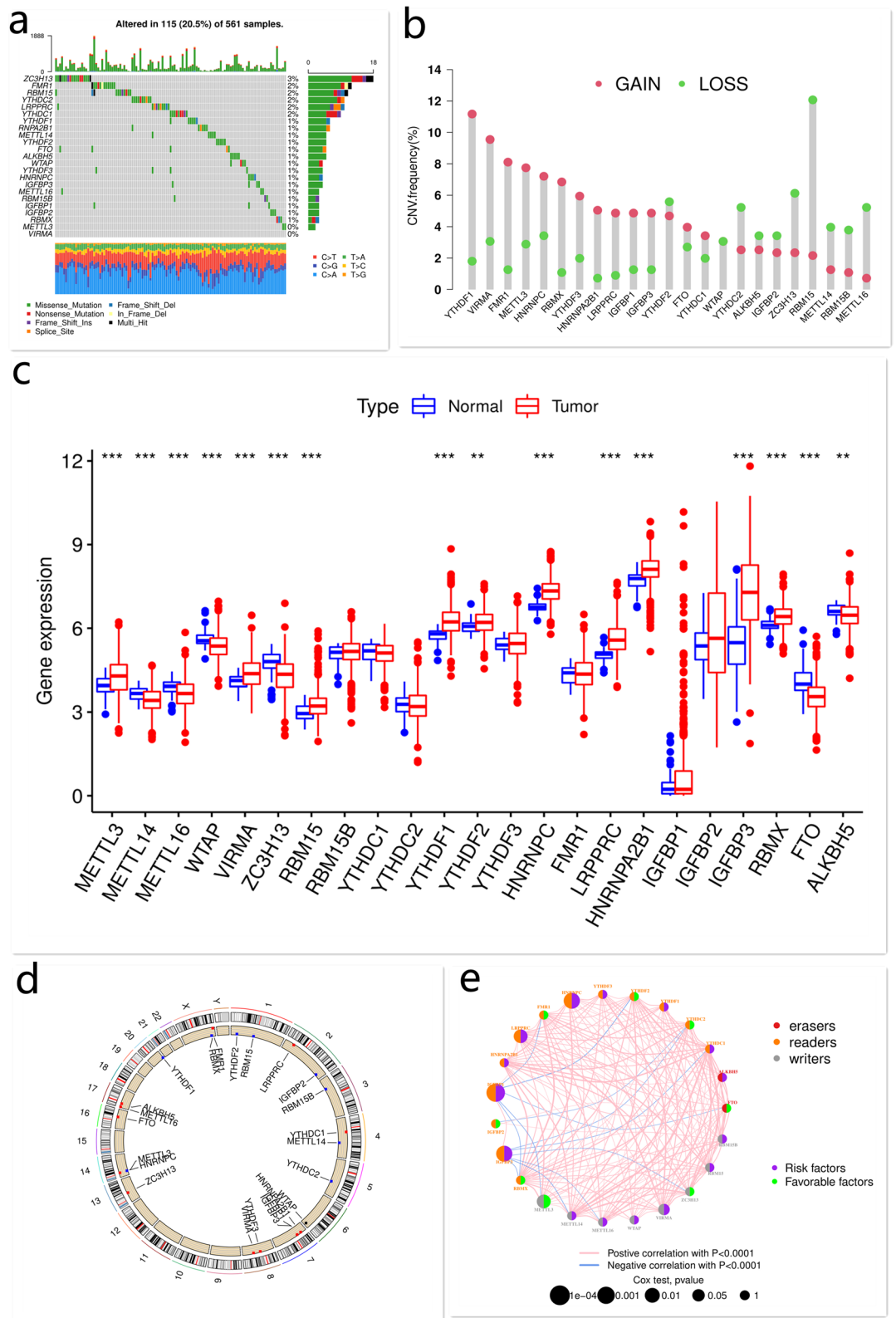


Figure 1. The expression, mutation characteristics, and relation of m⁶A regulators in LUAD. The mutation frequency of m⁶A regulators in LUAD (a). The CNV frequency of m⁶A regulators in LUAD. Blue dots indicate deletion frequency, while red dots indicate amplification frequency (b). The expression of m⁶A regulators in LUAD (c). The location of CNV alteration of 23 m⁶A regulators on chromosomes (d). The relation of m⁶A regulators in LUAD. The circle size indicates the survival impact of each m⁶A regulator. The lines connecting m⁶A regulators indicate their relations. The thickness of line indicates the strength of the relation. The red lines indicate positive relations, while the blue lines indicate negative relations (e). This figure is created using the R (version 4.0.3) (<https://www.r-project.org/>).

sues, the expressions of METTL3, VIRMA, RBM15, YTHDF1, YTHDF2, HNRNPC, LRPPRC, HNRNPA2B1, IGFBP3, and RBMX were markedly elevated in LUAD tissues, and vice versa (e.g. METTL14, METTL16, WTAP, ZC3H13, FTO, and ALKBH5) (Fig. 1c). The location of CNV alteration of m⁶A regulators on chromosomes is shown in Fig. 1d. These findings showed high genetic and expressional heterogeneity of m⁶A regulators between LUAD and normal lung tissues, suggesting that aberrant expression of m⁶A regulators may play a critical role in the occurrence and development of LUAD.

M⁶A modification-related patterns mediated by 23 m⁶A regulators. Three GEO datasets (GSE68465, GSE68571, and GSE72094) with available clinical information and overall survival (OS) data were integrated into one meta-cohort. A m⁶A regulator network was generated to depict the landscape of m⁶A regulator interactions and their prognostic value for LUAD (Fig. 1e; Supplementary Fig. S1). The m⁶A regulators in the same functional category were significantly correlated. We also observed significant correlations among “readers”, “writers”, and “erasers”. HNRNPC, YTHDF3, YTHDF1, YTHDC1, ALKBH5, RBM15B, RBM15, VIRMA, WTAP, METTL16, METTL14, IGFBP3, IGFBP1, HNRNPA2B1, and LRPPRC were the risk factors for LUAD. In addition, IGFBP1, HNRNPC, IGFBP3, and LRPPRC were significantly associated with the prognosis of LUAD patients (Fig. 1e, Supplementary Fig. S1). Considering that some m⁶A regulators (e.g. ZC3H13, FMR1, RBM15, YTHDC2, LRPPRC, and YTHDC1) had a relatively high mutation frequency, we compared the expression of mutant and wild-type m⁶A regulators. Compared with mutant-type tumors, the levels of WTAP, IGFBP2, and IGFBP1 in tumors with normal FMR1, LRPPRC, and YTHDC2 expression, respectively, were upregulated. Compared with wild-type tumors, the levels of LRPPRC and HNRNPA2B1 were upregulated in RBM15 and YTHDC1-mutant tumors, respectively (Supplementary Fig. S2a–e). The above data suggested that the cross-talk among these regulators plays a critical role in the occurrence, development, and prognosis of LUAD.

Three m⁶A modification-related patterns based on the expression of 23 m⁶A regulators were identified and termed m⁶A cluster-A–C, respectively (Supplementary Fig. S2f). Patients were then classified into different groups according to their m⁶A modification-related patterns (m⁶A cluster-A: n = 646; m⁶A cluster-B: n = 262; m⁶A cluster-C: n = 522). M⁶A cluster A was characterized by the upregulation of METTL14, RBM15, YTHDC1, YTHDC2, FMR1, and HNRNPA2B1; m⁶A cluster B showed upregulated expression of IGFBP1 and IGFBP3; m⁶A cluster C exhibited significantly increased expression of RBM15B, YTHDF2, IGFBP2, FTO, and ALKBH5 (Fig. 2a). Furthermore, a prominent survival advantage was observed in patients with m⁶A cluster-A and -C, while the worst survival was observed in those with m⁶A cluster-B (Fig. 2b). We also noticed that the percentage of patients with stage III and IV LUAD in m⁶A cluster-B was higher than that in m⁶A cluster-A and -C (Fig. 2c,d, Supplementary Table S1). Therefore, patients with m⁶A cluster-B had the worst survival and most advanced tumor stages compared to those with m⁶A cluster-A and C. Further analysis showed that the transcriptional profile of m⁶A cluster-B was significantly distinct from that of m⁶A cluster-A and -C, which was consistent with the clinical features (e.g. clinical survival and tumor stage) of patients with different m⁶A modification-related patterns (Supplementary Fig. S3a). The above results showed that m⁶A modification played a crucial role in the progression and prognosis of LUAD.

Characteristics of TME infiltration in different m⁶A modification-related patterns. The GSVA enrichment analysis was performed to explore the biological behaviors of different m⁶A modification-related patterns. In m⁶A cluster-A, the enriched pathways were associated with immune activation, such as cell adhesion molecules, T cell receptor signaling pathway, and natural killer cell-mediated cytotoxicity. Patients with m⁶A cluster-B presented poor survival and the enriched pathways were associated with carcinogenic activation, including NOD-like receptor signaling pathway and p53 signaling pathway. M⁶A cluster-C was predominantly related to sugar, lipid, and protein metabolism, such as fatty acid metabolism, N glycan biosynthesis, valine leucine and isoleucine degradation, and the TCA cycle (Fig. 2e–g, Tables 2, 3, 4). Surprisingly, m⁶A cluster-A was remarkably rich in TME-infiltrating immune cells, including T follicular helper cells, eosinophils, activated B cells, activated CD8 T cells, activated dendritic cells, immature B cells, mast cells, natural killer cells, macrophages, monocytes, plasmacytoid dendritic cells, myeloid-derived suppressor cells, and Type 1 T helper cells (Fig. 3a). Patients with m⁶A cluster-A also showed a survival advantage.

Establishment of m⁶A phenotype-gene signature and functional annotations. To investigate the biological behavior of different m⁶A modification-related patterns, we identified 810 m⁶A phenotype-related DEGs using the “limma” package (Supplementary Fig. S3b). The GO and KEGG³⁵ enrichment analyses for the DEGs were performed by the “clusterProfiler” package. The significantly enriched biological processes are shown in Supplementary Tables S2 and S3. The DEGs were closely related to immunity, implying that m⁶A modification played a vital role in tumor immune regulation. The immunity-related biological processes included positive regulation of PD-L1 expression, T cell activation, leukocyte activation, Th1 and Th2 cell differentiation, Th17 cell differentiation, PD-1 checkpoint pathway in cancer, etc. (Fig. 3b,c). To validate this finding, unsupervised clustering analysis based on 810 m⁶A phenotype-related genes was performed. Patients were then classified into different genomic subgroups. Consistent with the grouping by m⁶A modification-related patterns, three distinct m⁶A modification genomic phenotypes were identified using the unsupervised clustering algorithm, named m⁶A genecluster-A–C, respectively. There were 467 cases in m⁶A genecluster-A, 281 cases in m⁶A genecluster-B, and 682 cases in m⁶A genecluster-C (Supplementary Fig. S3c). Further analysis showed that patients with m⁶A cluster-B and the poorest survival were mainly assigned to m⁶A genecluster-A and -B, while those with m⁶A cluster-A/-C and survival advantages were mainly assigned to m⁶A genecluster-C (Figs. 2c, 3d; Supplementary Table S1). Patients with stage I and II LUAD were mainly characterized by m⁶A genecluster-C, which was proven to be related to a better prognosis, while those with stage III and IV LUAD were characterized by m⁶A

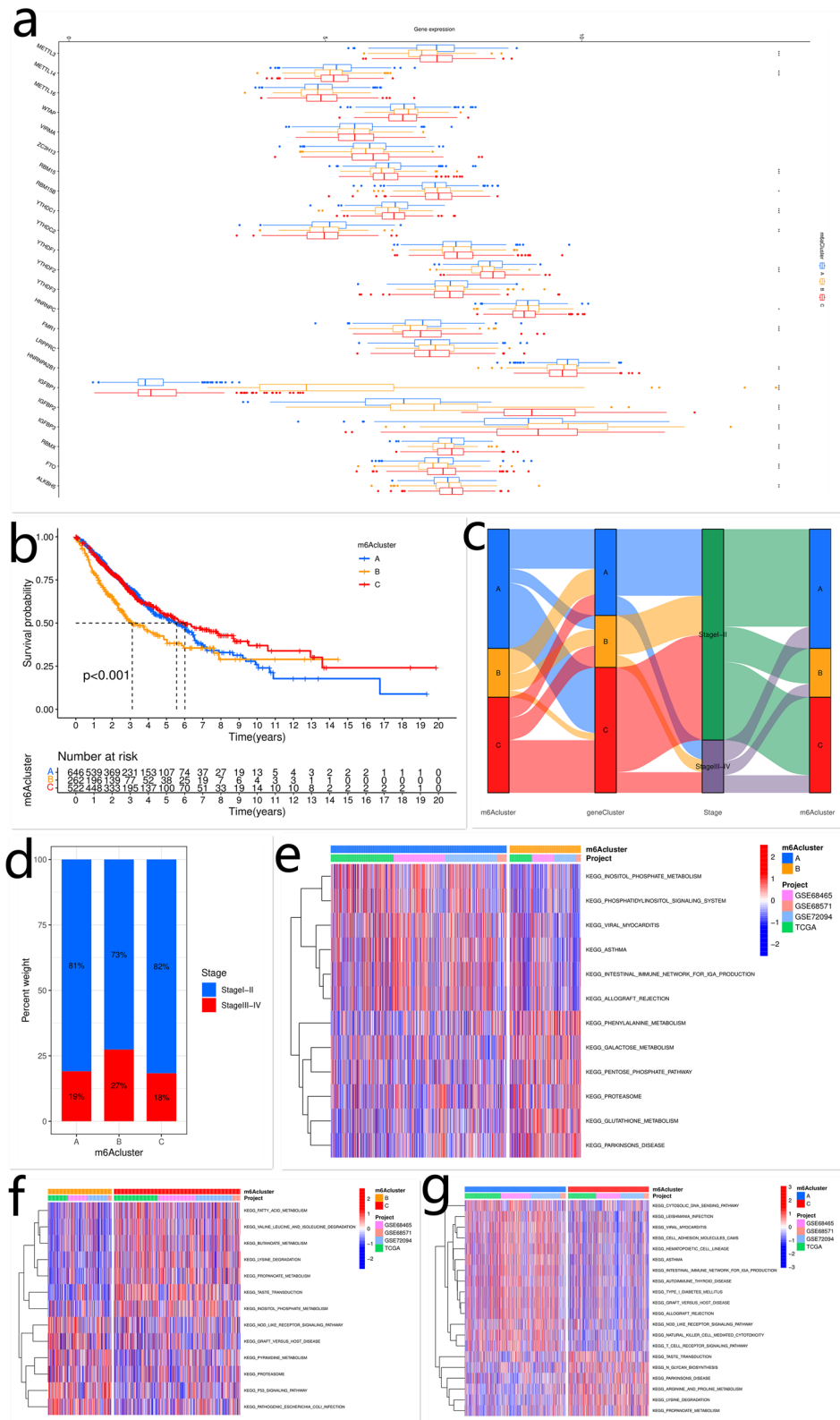


Figure 2. The expression of m⁶A regulators, clinical characteristics of LUAD patients, and biological processes in different m⁶A modification-related patterns. The expression of m⁶A regulators in different m⁶A modification-related patterns (a). The Kaplan–Meier curves of the OS of LUAD patients with different m⁶A modification-related patterns (b). The relationships among m⁶A cluster, m⁶A genecluster, and stage were visualized using alluvial diagram (c). The percentage of patients with stage I, II/III, and IV LUAD in each m⁶A cluster (d). The biological processes in different m⁶A modification-related patterns. Red indicates activation, while blue indicates inhibition (e, f, g). This figure is created using the R (version 4.0.3) (<https://www.r-project.org/>).

Pathway	logFC	AveExpr	t	p value	Adj. p val.
Glutathione metabolism	0.165641	- 0.02904	8.208943	7.21E-16	1.14E-13
Inositol phosphate metabolism	- 0.12199	- 0.00484	- 7.71161	3.12E-14	2.47E-12
Phosphatidylinositol signaling system	- 0.10869	0.002708	- 7.19802	1.24E-12	6.52E-11
Phenylalanine metabolism	0.138609	- 0.03086	6.801562	1.83E-11	7.21E-10
Asthma	- 0.1507	0.048538	- 6.3068	4.35E-10	8.60E-09
Parkinsons disease	0.127406	- 0.05194	6.105625	1.49E-09	2.35E-08
Viral myocarditis	- 0.10773	0.054209	- 5.85274	6.65E-09	9.55E-08
Galactose metabolism	0.101446	0.012333	5.52438	4.27E-08	4.08E-07
Pentose phosphate pathway	0.111034	- 0.0334	5.519075	4.39E-08	4.08E-07
Intestinal immune network for IGA production	- 0.10316	0.058451	- 3.9643	7.91E-05	0.000278
Allograft rejection	- 0.10911	0.068016	- 3.9402	8.74E-05	0.0003
Proteasome	0.103781	- 0.00538	3.913471	9.75E-05	0.000328

Table 2. The activation states of biological pathways in distinct m⁶A modification patterns by GSVA enrichment analysis (A vs. B). AveExpr: average expression; adj. p. val: adjust p value.

Pathway	logFC	AveExpr	t	p value	Adj. p val.
Taste transduction	0.173708	0.023282	9.54949	1.48E-20	2.33E-18
Lysine degradation	0.176431	0.022864	8.486039	1.00E-16	7.91E-15
Valine leucine and isoleucine degradation	0.165508	0.00292	7.31964	5.96E-13	3.14E-11
P53 signaling pathway	- 0.10236	- 0.00466	- 6.907	9.97E-12	3.94E-10
Inositol phosphate metabolism	0.100877	- 0.02475	6.540024	1.08E-10	3.15E-09
Pathogenic Escherichia coli infection	- 0.11322	- 0.02392	- 6.52473	1.20E-10	3.15E-09
Propanoate metabolism	0.159995	0.012698	6.401749	2.59E-10	5.85E-09
Butanoate metabolism	0.136867	0.00647	6.275974	5.64E-10	1.09E-08
Nod like receptor signaling pathway	- 0.10518	- 0.0319	- 5.96341	3.68E-09	5.28E-08
Pyrimidine metabolism	- 0.10614	- 0.01397	- 5.65029	2.21E-08	2.91E-07
Fatty acid metabolism	0.122256	0.006	5.269864	1.75E-07	1.84E-06
Proteasome	- 0.11058	- 0.00488	- 4.13551	3.91E-05	0.000199
Graft versus host disease	- 0.10532	- 0.06268	- 3.57728	0.000368	0.00132

Table 3. The activation states of biological pathways in distinct m⁶A modification patterns by GSVA enrichment analysis (B vs. C). AveExpr: Average expression, t, adj.P.Val: adjust P Value.

genecluster-A and -B, with a poorer clinical outcome (Figs. 2c, 3e–f; Supplementary Table S1). These results further confirmed that m⁶A modification played a crucial role in the progression and prognosis of LUAD. In these m⁶A gene clusters, differential expression of m⁶A regulators was observed. M⁶A genecluster-A was characterized by upregulated expression of WTAP and IGFBP3; m⁶A genecluster-B showed increased expression of RBM15B, YTHDF3, LRPPRC, HNRNPC, IGFBP1, IGFBP2, and ALKBH5; m⁶A genecluster-C exhibited significantly increased expression of METTL3, METTL14, RBM15, YTHDC1, YTHDC2, YTHDF2, FMR1, RBMX, and FTO (Fig. 3g).

Clinical and transcriptome characteristics of three m⁶A modification-related patterns. The above results suggested that m⁶A modification played a key regulatory role in shaping the TME landscape. However, these data were based on the patient population, not at the individual level. Considering the complexity and heterogeneity of m⁶A modification in different individuals, a scoring system was developed based on m⁶A phenotype-related genes to quantify the m⁶A modification-related pattern of each patient, and the results were shown as the m⁶Ascore. The alluvial diagram was used to visualize the attribute changes of each individual (Fig. 4a). The Kruskal–Wallis test showed significant differences in the m⁶Ascore among different m⁶A gene clusters. M⁶A genecluster-C was related to a better prognosis and showed a higher median score compared with m⁶A genecluster-A and -B (Fig. 4b). In addition, m⁶A cluster-A and -C showed significantly increased m⁶Ascore compared with m⁶A cluster-B (Fig. 4c). Previous analysis demonstrated that patients with m⁶A cluster-A had a survival advantage and this pattern was remarkably rich in infiltrating immune cells, indicating that high m⁶Ascore may be correlated with immune activation-related signature and survival advantage. To better elucidate the characteristics of the m⁶A signature, we examined the correlation between the m⁶Ascore and TME-infiltrating immune cells in LUAD (Fig. 4d). The results showed that high m⁶Ascore was significantly correlated with immune activation.

To evaluate the prognostic value of the m⁶Ascore for patients' outcomes, LUAD patients were classified into the low and high m⁶Ascore groups with the cut-off value determined by the "survminer" R package. Next, we

Pathway	logFC	AveExpr	t	P.Value	adj.P.Val
Natural killer cell mediated cytotoxicity	-0.13661	0.013288	-10.3918	2.70E-24	4.27E-22
Lysine degradation	0.151444	-0.00211	9.616063	3.77E-21	2.98E-19
Arginine and proline metabolism	0.111808	-0.01228	9.110563	3.28E-19	1.73E-17
Graft versus host disease	-0.19841	0.012295	-8.72385	8.68E-18	2.74E-16
Allograft rejection	-0.18999	0.015054	-8.69579	1.10E-17	2.89E-16
Leishmania infection	-0.13862	0.012236	-8.5997	2.42E-17	5.47E-16
Viral myocarditis	-0.1303	0.027342	-8.43941	8.94E-17	1.47E-15
Nod like receptor signaling pathway	-0.11469	-0.00344	-8.43444	9.31E-17	1.47E-15
T cell receptor signaling pathway	-0.10918	0.008681	-8.16473	7.98E-16	9.70E-15
Cytosolic DNA sensing pathway	-0.11416	0.00249	-8.05372	1.90E-15	2.14E-14
Type I diabetes mellitus	-0.14067	0.005598	-7.76164	1.77E-14	1.74E-13
Asthma	-0.14966	0.025435	-7.64815	4.12E-14	3.83E-13
Taste transduction	0.105965	0.022686	7.616596	5.21E-14	4.33E-13
Intestinal immune network for IGA production	-0.15357	0.019942	-7.40868	2.38E-13	1.79E-12
Parkinsons disease	0.116117	-0.03703	7.038527	3.24E-12	2.13E-11
Autoimmune thyroid disease	-0.12703	0.016094	-6.86282	1.07E-11	6.78E-11
Hematopoietic cell lineage	-0.10746	0.017027	-6.79882	1.65E-11	1.00E-10
N-glycan biosynthesis	0.101026	-0.01521	6.612347	5.65E-11	3.30E-10
Propanoate metabolism	0.12416	-0.00262	6.549583	8.49E-11	4.79E-10
Cell adhesion molecules cams	-0.10653	0.022996	-6.53179	9.52E-11	5.19E-10
Primary immunodeficiency	-0.14419	0.008395	-6.46014	1.51E-10	7.95E-10
Citrate cycle TCA cycle	0.101751	-0.02543	5.872817	5.52E-09	2.57E-08

Table 4. The activation states of biological pathways in distinct m⁶A modification patterns by GSVA enrichment analysis (A vs. C). AveExpr: average expression, adj. *p* val: adjust *p* value.

investigated whether the m⁶Ascore was an independent prognostic biomarker for LUAD. The univariate and multivariate Cox regression model analyses, which included the clinical and demographic factors of patients (i.e. gender, age, and TNM stage), confirmed that the m⁶Ascore was an independent and robust prognostic marker for the outcome of LUAD patients and was inversely associated with the risk of LUAD (Fig. 4e,f). Further analysis showed that patients with a high m⁶Ascore had a significant survival benefit, which was consistent with the above results (Fig. 5a–c). To further assess the stability of the m⁶Ascore model, the prognostic value of the risk score for LUAD patients with different clinical characteristics, including age, gender, and TNM stage, was evaluated (Supplementary Fig. S4a–f). The results also showed that high m⁶Ascore was correlated with a better clinical benefit. In addition, we examined whether the combination of the m⁶Ascore and the mutation signatures of m⁶A regulators could predict the survival of patients with LUAD. We found that patients with high m⁶Ascore and mutation frequency had a better prognosis, while those with low m⁶Ascore and mutation frequency experienced poor outcomes (Fig. 5d). The other result obtained from this analysis was that patients with a high m⁶Ascore always showed a survival advantage, independent of the mutation frequency (Fig. 5d).

Characteristics of m⁶A modification in tumor somatic mutation. The difference in the distribution of somatic mutation between high and low m⁶Ascore groups in the TCGA-LUAD cohort was analyzed using the “maftools” package. The low m⁶Ascore group showed more extensive TMB compared with patients with a high m⁶Ascore (rate of all mutated gene: 96.08% vs. 86.48%) (Figs. 5e,f, 6a,b). The TMB quantification analysis showed that the m⁶Ascore and TMB were negatively correlated.

The role of m⁶A modification-related patterns in anti-CTLA4 immunotherapy. The anti-CTLA4 and anti-PD-1 immunotherapies have emerged as promising options for cancer therapy. We examined whether the m⁶A modification-related pattern could predict the response of patients to anti-CTLA4 and anti-PD-1 therapies. Patients treated with anti-CTLA4 immunotherapy exhibited significant clinical benefits (Fig. 6c–e). In addition, compared to the low m⁶Ascore group, patients with a high m⁶Ascore showed significant therapeutic advantage and better clinical response to anti-CTLA4 therapy (Fig. 6d). Patients with a high m⁶Ascore also showed upregulated expressions of B7-1 (CD80) and B7-2 (CD86), indicating a potential response to anti-CTLA4 therapy (Fig. 6f,g). These data implied that the m⁶Ascore was a robust biomarker for predicting the clinical response and prognosis of LUAD patients. Taken together, our study showed that m⁶A modification-related patterns were significantly correlated with tumor immune phenotypes and clinical response to anti-CTLA4 therapy. The established m⁶A modification-related signature may be used to predict the response of LUAD patients to anti-CTLA4 immunotherapy.

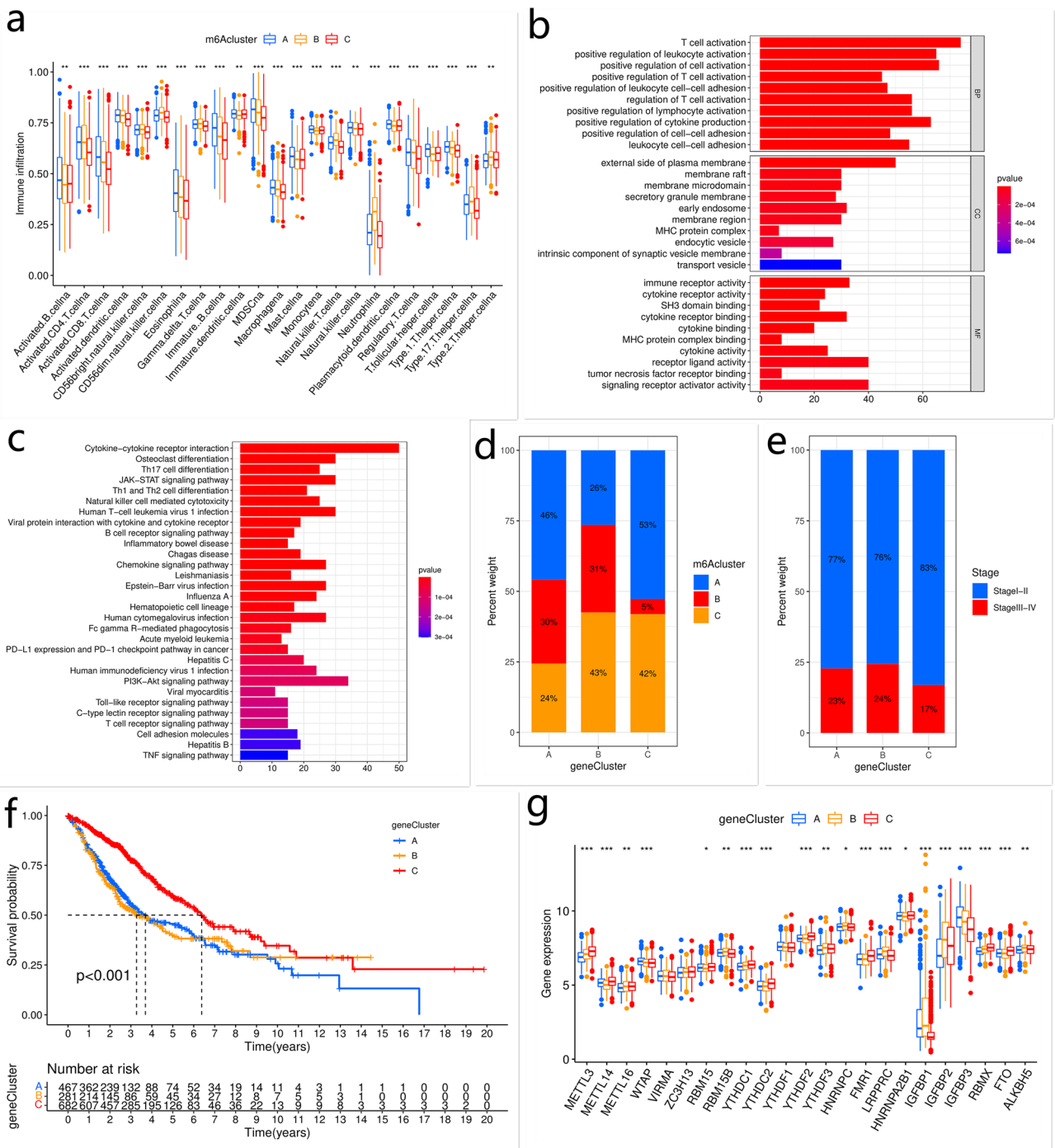


Figure 3. TME-infiltrating immune cells in different m6A modification-related patterns; biological processes and clinical characteristics of LUAD patients in different m6A geneclusters. Characteristics of TME-infiltrating cells in different m6A modification-related patterns (a). GO and KEGG enrichment analyses of m6A phenotype-related DEGs (b, c). The percentage of patients with m6A cluster A/B/C in each m6A geneCluster (d). The percentage of patients with stage I, II/III, and IV LUAD in each m6A geneCluster (e). The Kaplan-Meier curves of the OS of LUAD patients in different m6A geneClusters (f). The expression of m6A regulators in distinct m6A geneclusters (g). This figure is created using the R (version 4.0.3) (<https://www.r-project.org/>).

Discussion

As the most common RNA modification, m6A methylation plays an important role in post-transcriptional regulation^{22,36}. Aberrant m6A modification is closely associated with the onset and development of cancers^{22,23}. Increasing evidence has shown that m6A modification plays a key role in TME infiltration of immune cells and tumor immunotherapy. However, the mechanisms by which m6A modification affects TME infiltration and immunotherapy have not been fully elucidated. Moreover, previous studies mainly focused on a single TME

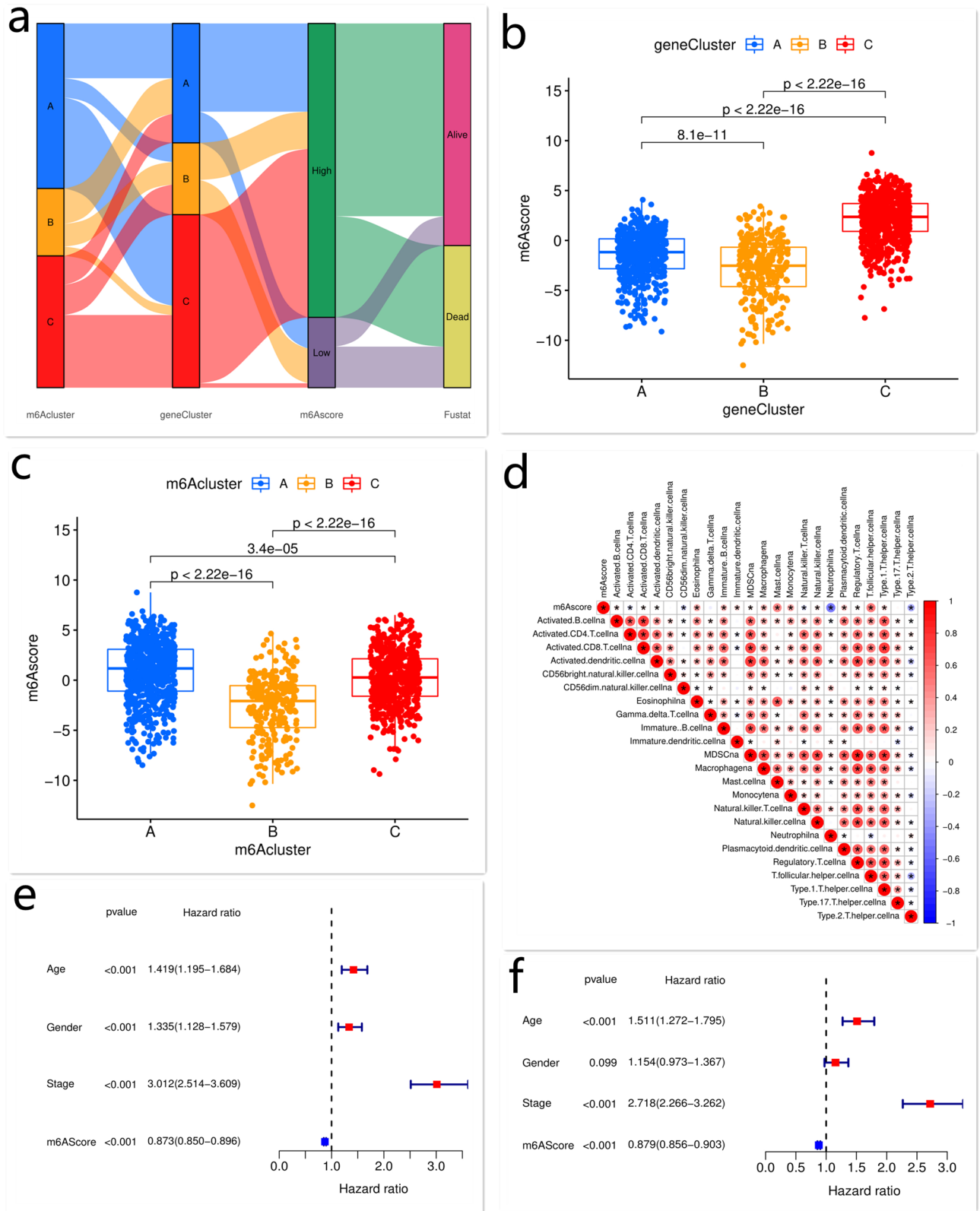


Figure 4. The relationships between the m⁶Ascore and molecular characteristics. The relationships among m⁶A cluster, m⁶A genecluster, survival status (Fustat), and m⁶Ascore were visualized using the alluvial diagram (a). The m⁶Ascore in different m⁶A genecluster and m⁶A cluster was obtained by the Kruskal–Wallis test (b, c). The correlation between TME-infiltrating immune cells and the m⁶Ascore in LUAD (d). Univariate and multivariate analyses of the m⁶Ascore (e, f). This figure is created using the R (version 4.0.3) (<https://www.r-project.org/>).

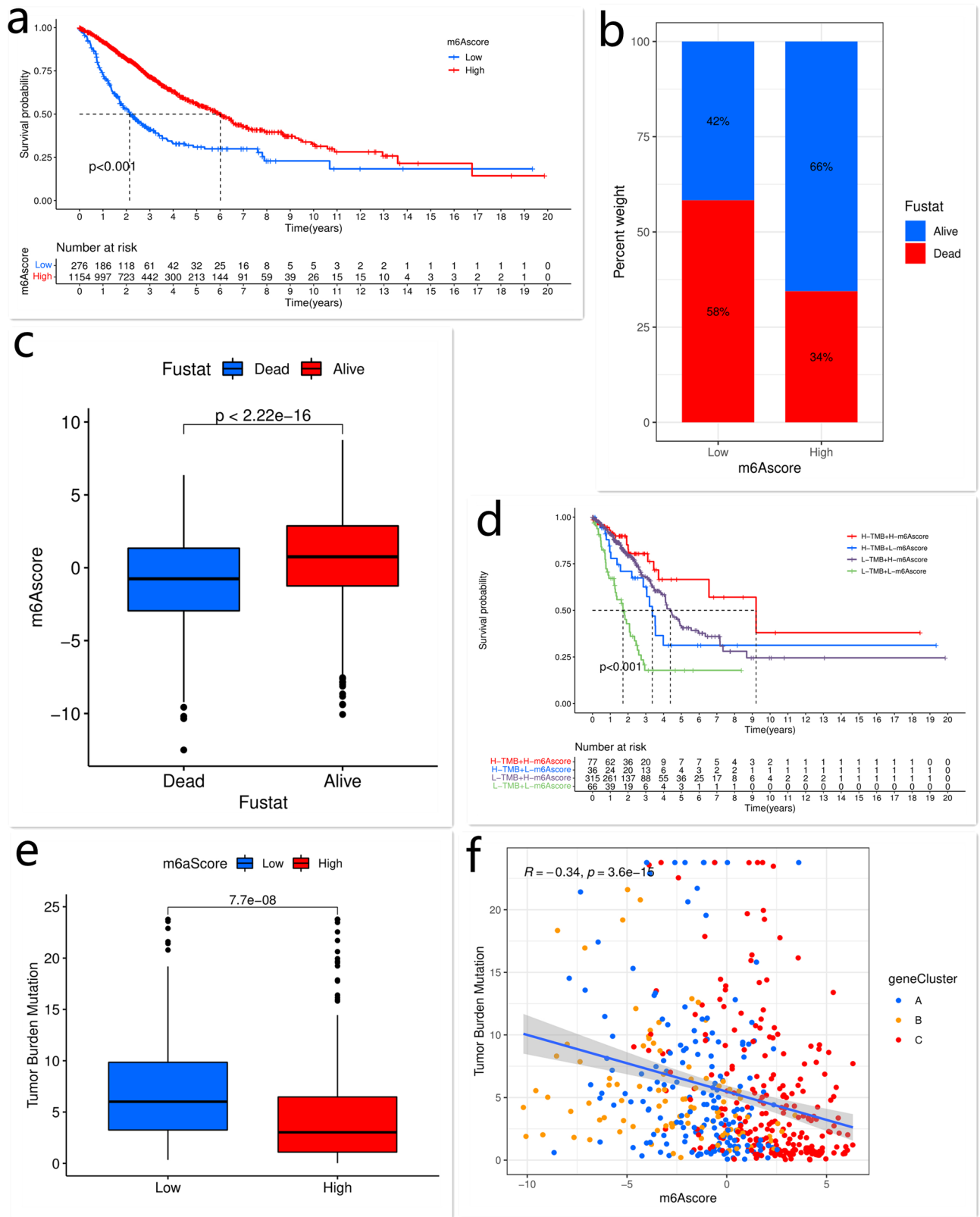


Figure 5. The correlations of the m⁶Ascore with clinical characteristics and TMB. The Kaplan–Meier curves of the OS of LUAD patients with low or high m⁶Ascore (a). The correlation between the m⁶Ascore and survival status (Fustat) of patients (b, c). The Kaplan–Meier curves of the OS of subgroup patients stratified by the m⁶Ascore and TMB (d). The relationship between the m⁶Ascore and TMB (e, f). This figure is created using the R (version 4.0.3) (<https://www.r-project.org/>).

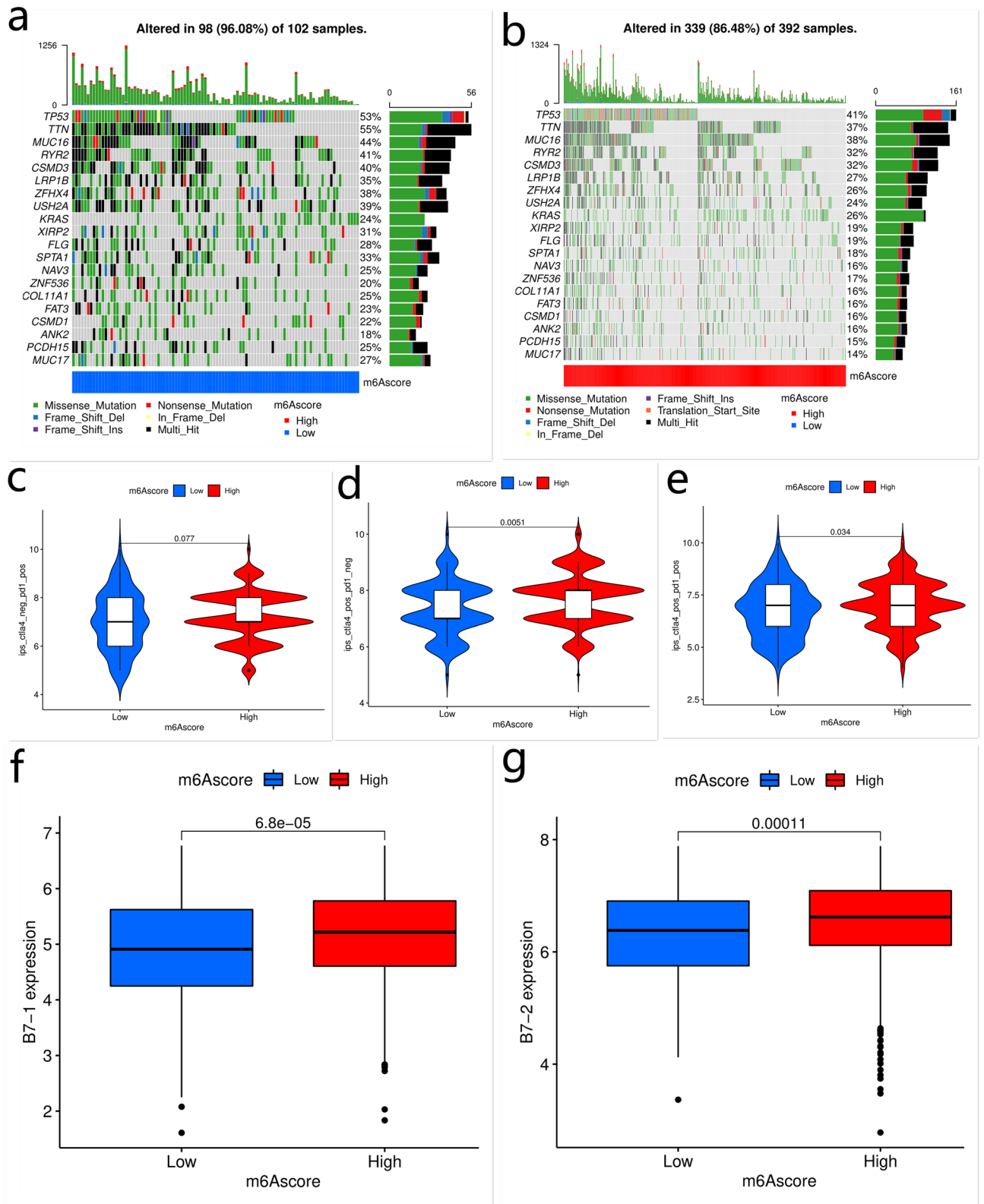


Figure 6. The frequency of all mutated gene and immunotherapeutic response of patients with low or high m⁶Ascore. The frequency of all mutated genes in LUAD in the low and high m⁶Ascore groups (a,b). The effectiveness of anti-CTLA4 and/or anti-PD-1 immunotherapies in the low and high m⁶Ascore groups. “ctla4-neg-pd1-pos” indicates patients treated with anti-PD-1 therapy alone; “ctla4-pos-pd1-neg” indicates patients treated with anti-CTLA4 therapy alone; “ctla4-pos-pd1-pos” indicates patients treated with both anti-CTLA4 and anti-PD-1 therapies (c-e). The expressions of B7-1 and B7-2 in the low and high m⁶Ascore groups (f,g). This figure is created using the R (version 4.0.3) (<https://www.r-project.org/>).

cell type or regulator. The regulatory effects of multiple m⁶A regulators on the overall characteristics of TME infiltration in LUAD warrant further investigation.

In this study, we identified three distinct m⁶A modification-related patterns with significantly distinct biological characteristics by 23 m⁶A regulators. Patients with m⁶A cluster-A showed a survival advantage and the enriched pathways were associated with immune activation. Patients with m⁶A cluster-B had poor survival and the enriched pathways were associated with carcinogenic activation. The pathways enriched in patients with m⁶A cluster-C were related to substance metabolism. In addition, m⁶A cluster-A was remarkably rich in TME-infiltrating immune cells. These findings were consistent with a previous study, showing that an imbalanced immune system played a pivotal role in tumor progression^{13,37}. LUAD is an immunosuppressive disorder that is implicated in TME cell infiltration^{14,38}. Cancer patients with abundant TME-infiltrating immune cells showed a survival advantage^{39,40}. TME is regulated by various immunoregulatory signals that are involved in the initiation, development, and metastasis of LC, and its heterogeneity may lead to multiple dimensions in the therapeutic response and prognosis of patients^{11,12,41,42}. A previous study reported that immunotherapy promoted the therapeutic effects of NSCLC treatment by activating the host immune system and regulating TME⁴³. In this study, by analyzing TME infiltration and survival outcome of each cluster, we validated the reliability of immune phenotype classification for distinct m⁶A modification-related patterns. These findings suggested that TME-infiltrating immune cells protected against LUAD and had an effect on LUAD immunotherapy.

Next, the DEGs in distinct m⁶A modification-related patterns were identified, referring to m⁶A phenotype-related genes. Based on these DEGs, patients with LUAD were divided into three groups. Further analysis showed that the DEGs were closely related to immunity, indicating that m⁶A modification plays a vital role in the classification of TME. The characteristics of TME-infiltrating immune cells in LUAD were further investigated by a comprehensive assessment of m⁶A modification-related patterns. Considering the heterogeneity and complexity of m⁶A modification in different individuals, a scoring system was developed to quantify the m⁶A modification-related pattern of each patient, and the results were shown as the m⁶Ascore. The m⁶A modification-related pattern that was rich in infiltrating immune cells was characterized by significantly increased m⁶Ascore and survival advantage. The univariate and multivariate Cox regression model analyses identified the m⁶Ascore as an independent prognostic marker for the outcome of LUAD patients. Additionally, the m⁶Ascore was a reliable prognostic factor for LUAD patients with different clinical characteristics, including gender, age, and TNM stage. These data suggest that the m⁶Ascore may be used to comprehensively assess individual m⁶A modification-related pattern and therefore to determine TME infiltration pattern, that is, tumor immune phenotype. Further analysis revealed that the high m⁶Ascore group had lower TMB than the low m⁶Ascore group. The missense mutation is closely related to immunotherapy⁴⁴. The study by Samstein et al. found that patients with higher somatic TMB had better immunotherapy responses⁴⁵. The mutation is also related to the activation of immune cells. HNSCC patients with low TMB had increased numbers of CD⁴⁺ memory resting cells and B memory cells, as well as a better prognosis⁴⁶.

Although anti-CTLA4 and anti-PD-1 immunotherapies have emerged as promising approaches for treating LUAD, especially advanced LUAD, individual heterogeneity remains a critical challenge. Therefore, it is of great importance to identify novel markers that could predict the outcomes of immunotherapies. In this study, we showed that m⁶A modification significantly affected the TME landscape in LUAD, implying that the therapeutic efficacy of immunotherapy may be affected by m⁶A modification. Additionally, patients treated with anti-CTLA4 immunotherapy exhibited significant clinical benefits. Patients with a high m⁶Ascore showed significant therapeutic advantage and better clinical response to anti-CTLA4 therapy. Meanwhile, Patients with high m⁶Ascores also showed upregulated expressions of B7-1 and B7-2. Previous studies have reported that CTLA-4 was a negative regulator of T cell activation. The binding of CTLA-4 to B7-1 and B7-2 ligands inhibited T cell activation. Meanwhile, anti-CTLA4 immunotherapy augments antitumor responses by inhibiting B7-1 and B7-2 ligands of T cells^{47–49}. Here, we showed that m⁶A modification significantly affected the response of LUAD patients to immunotherapy and the m⁶Ascore was a predictor of clinical response to anti-CTLA4 immunotherapy in this population.

Our study provided a new perspective of individualized immunotherapy and immuno-oncology for LUAD. However, some limitations of the current study need to be addressed. The data were obtained from TCGA and GEO databases. Due to insufficient clinical cohort, the proposed model and interactions among m⁶A modification, TME, and immunotherapy, warrant clinical verification. Future large-cohort, prospective clinical trials are needed.

Conclusions

This study showed the regulatory mechanisms of m⁶A modification on TME in LUAD patients. The response of patients with different m⁶Ascore to immunotherapy was comprehensively assessed. Our findings may contribute to the improvement of current immunotherapy and the development of individualized immunotherapy for LUAD patients.

Methods

Data source and preprocessing. The workflow of our study was shown in Fig. 7. The RNA sequencing transcriptome of LUAD patients and corresponding clinical data were obtained from TCGA (<https://portal.gdc.cancer.gov/>) and GEO (<https://www.ncbi.nlm.nih.gov/geo/>) databases. Patients without survival information were excluded. A total of four eligible LUAD cohorts (GSE68465, GSE68571, GSE72094, and The Cancer Genome Atlas-Lung Adenocarcinoma (TCGA-LUAD)) were gathered for further analyses. The R (version 4.0.3) (<https://www.r-project.org/>) and R Bioconductor packages (<https://www.bioconductor.org/>) were used for data analysis. For the TCGA datasets, the RNA sequencing data (FPKM value) obtained from the Genomic Data

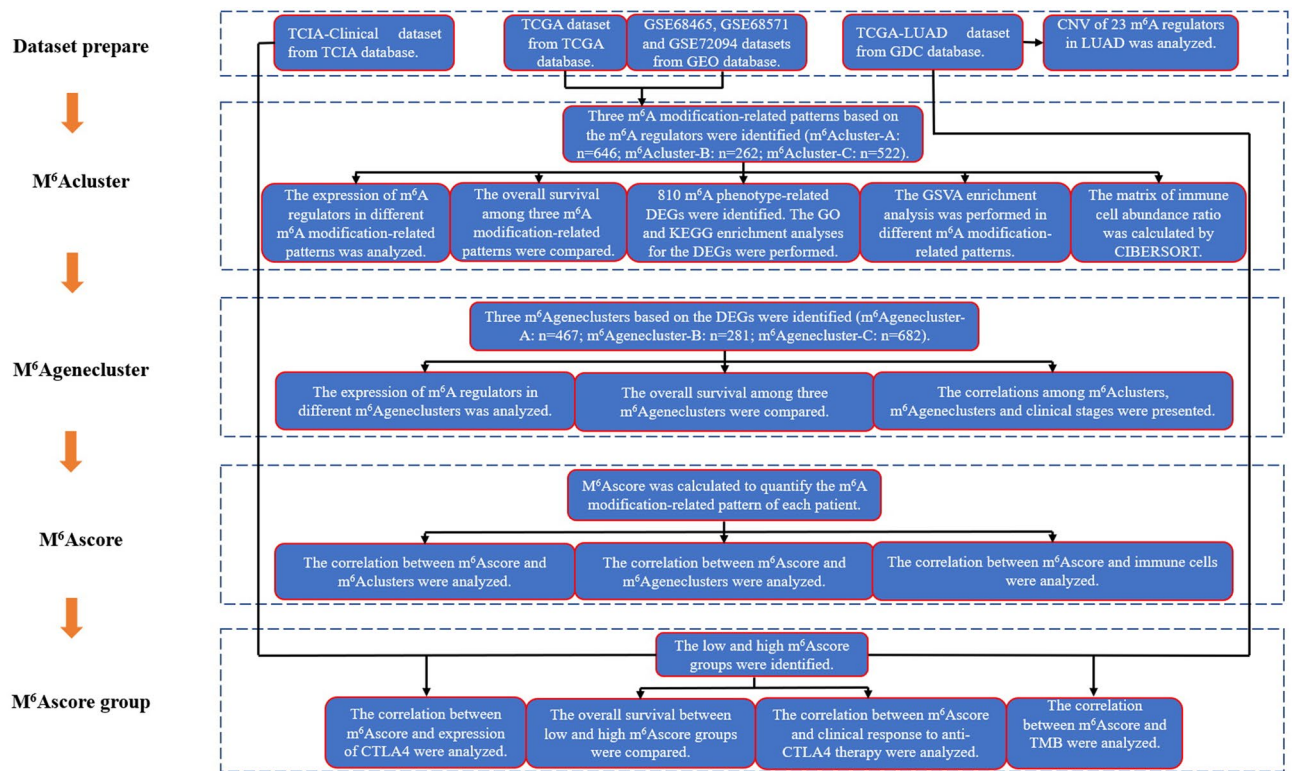


Figure 7. The workflow of our study.

Commons (GDC) were transformed into transcripts per kilobase million (TPM) values. The somatic mutation data obtained from TCGA were used to demonstrate the mutation frequency of m⁶A regulators in LUAD using the “maftools” R package. The copy number variation (CNV) data obtained from UCSC Xena (<https://xena.ucsc.edu/>) database were used for Copy Number Variation analysis using the R (version 4.0.3). The baseline information of LUAD patients on the datasets of our study was shown in Table 5.

Unsupervised clustering for 23 m⁶A regulators. A total of 23 m⁶A regulators were collected from previous studies (Table 1). To determine their biological and functional characteristics in LUAD, unsupervised clustering algorithm was used to categorize LUAD patients according to their m⁶A modification-related patterns using the “ConsensusClusterPlus” package. This algorithm was applied 1000 times to ensure the stability of classification.

Gene set variation analysis (GSVA) and functional annotations. To investigate the biological processes and pathways in different m⁶A modification-related patterns, the “GSVA” R packages and “c2.cp.kegg.v6.2.symbols” gene sets were obtained for GSVA. A *p*-value of less than 0.05 indicated significantly enriched biological processes and pathways. The functional annotations of m⁶A-related genes were analyzed using the “clusterProfiler” R package. The cut-off value was set as a *p* < 0.05.

Estimation of TME infiltration. The relative abundance of TME-infiltrating cells in individual samples was yielded using the single-sample gene set enrichment analysis (ssGSEA). The enrichment score was obtained from the ssGSEA and differential immune cell infiltration among different subsets was analyzed.

Identification of differentially expressed genes (DEGs) among different m⁶A phenotypes. Patients were divided into three groups according to their m⁶A modification-related patterns. A *p*-value of < 0.05 was used to identify DEGs using the “Limma” R package.

Establishment of m⁶A phenotype-related gene signature. A scoring system was developed to quantify the m⁶A modification-related pattern of each patient and the m⁶A phenotype-related gene signature was termed the m⁶Ascore. The gene signature was established as follows: Unsupervised clustering algorithm was used to identify overlapped DEGs and then to divide patients into different subsets. To define the number of clusters and their stability, consensus clustering algorithm was applied. Then, a univariate Cox regression model was established to determine the prognostic value of each gene. The genes with significant prognostic value were extracted for further analyses. Subsequently, principal component analysis (PCA) was performed to establish the m⁶A phenotype-related gene signature. The m⁶Ascore was calculated using the following equation^{50,51}:

Characteristics	TCGA		GSE68465		GSE68571		GSE72094		TCIA-ClinicalData	
	Number of cases	Percentages (%)	Number of cases	Percentages (%)						
Sex										
Female	280	53.60	220	49.66	51	59.30	240	54.30	280	48.78
Male	242	46.40	223	50.34	35	40.70	202	45.70	242	42.16
Unknown	0	0.00	0	0.00	0	0.00	0	0.00	52	9.06
Age										
≤ 65	241	46.17	231	52.14	50	58.14	127	28.73	236	41.11
> 65	262	50.19	212	47.86	36	41.86	294	66.52	255	44.43
Unknown	19	3.64	0	0.00	0	0.00	21	4.75	83	14.46
Race										
White	–	–	295	66.59	–	–	399	90.27	393	68.47
Black	–	–	12	2.71	–	–	13	2.94	53	9.23
Unknown	–	–	136	30.70	–	–	30	6.79	128	22.30
Smoking										
Yes	–	–	300	67.72	74	86.05	335	75.79	356	62.02
No	–	–	49	11.06	9	10.46	33	7.47	0	0.00
Unknown	–	–	94	21.22	3	3.49	74	16.74	218	37.98
Survival time										
≤ 5 years	460	88.12	273	61.62	65	75.58	393	88.91	460	80.14
> 5 years	53	10.15	169	38.15	21	24.42	5	1.13	53	9.23
Unknown	9	1.73	1	0.23	0	0.00	44	9.96	61	10.63
Survival status										
Alive	334	64.98	207	46.73	62	72.09	298	67.42	334	58.19
Dead	188	36.02	236	53.27	24	27.91	122	27.60	197	34.32
Unknown	0	0.00	0	0.00	0	0.00	22	4.98	43	7.49
Stage										
Stage I	279	53.45	276	62.30	67	77.91	265	59.95	279	48.61
Stage II	124	23.76	95	21.44	0	0.00	69	15.61	124	21.60
Stage III	85	16.28	69	15.58	19	22.09	63	14.25	85	14.81
Stage IV	26	4.98	0	0.00	0	0.00	17	3.85	26	4.53
Unknown	8	1.53	3	0.68	0	0.00	28	6.34	60	10.45

Table 5. The baseline information of LUAD patients on the datasets of our study.

$$m^6 \text{Score} = \sum (PC1i + PC2i)$$

i indicates the expression of m^6A phenotype-related genes.

Data of immune-checkpoint blockade. To evaluate the therapeutic response of patients with distinct m^6A modification-related patterns to CTLA4 and PD-1 blockade therapies, the TCIA-Clinical Data of LUAD was downloaded from The Cancer Immunome Atlas (TCIA) database (<https://tcia.at/>). Four groups of patients were included in our study: (1) patients treated with both anti-PD-1 and anti-CTLA4 immunotherapies; (2) patients treated with anti-CTLA4 therapy but not anti-PD-1 therapy; (3) patients treated with anti-PD-1 therapy but not anti-CTLA4 therapy; (4) patients not treated with anti-PD-1 or anti-CTLA4 therapy. The immunotherapy score of each patient was obtained for further analysis. Then, the correlation between immunotherapy effectiveness and the m^6A Score was examined. The expression levels of B7-1 and B7-2 were also obtained from the above databases.

Statistical analysis. Spearman and distance correlation analyses were performed to assess the correlation between the expression of m^6A regulators and TME-infiltrating immune cells. Kruskal–Wallis tests and one-way ANOVA were used to compare the results among three or more subgroups. The “survminer” R package was used to calculate the cut-off point of each dataset subgroup according to the correlation between the m^6A Score and patients’ survival. The “surv-cutpoint” function, which repeatedly tested all potential cut points to find the one achieving the maximum rank statistic, was used to dichotomize the m^6A Score. Subsequently, patients were classified into the low and high m^6A Score groups using the maximally selected log-rank statistics to minimize the batch effect. The Kaplan–Meier method was applied to visualize the survival curves and log-rank tests were used to identify statistical significance. The univariate and multivariate Cox regression model analyses were used to identify independent prognostic factors. The forest plots of prognostic factors were generated using the

“forestplot” R package. The waterfall function of the “maftools” R package was used to demonstrate the mutation landscape of LUAD patients with low or high m⁶Ascore. The CNV landscape of 23 m⁶A regulators in 23 pairs of chromosomes was delineated using the “RCircos” R package. A *p*-value of less than 0.05 indicated statistical significance. The R (version 4.0.3) was used for data analysis.

Ethical approval. My study did not require ethical approval.

Data availability

The following information was supplied regarding data availability: The datasets are available at the TCGA (<https://portal.gdc.cancer.gov/>), GEO (<https://www.ncbi.nlm.nih.gov/geo/>), and TCIA (<https://tcia.at/>) databases.

Received: 3 June 2021; Accepted: 30 September 2021

Published online: 22 October 2021

References

- Siegel, R. L., Miller, K. D. & Jemal, A. Cancer statistics, 2019. *CA: A Cancer J. Clin.* **69**, 7–34. <https://doi.org/10.3322/caac.21551> (2019).
- Torre, L. A., Siegel, R. L. & Jemal, A. Lung cancer statistics. *Adv. Exp. Med. Biol.* **893**, 1–19. https://doi.org/10.1007/978-3-319-24223-1_1 (2016).
- Hirsch, F. R. *et al.* Lung cancer: current therapies and new targeted treatments. *Lancet* **389**, 299–311. [https://doi.org/10.1016/s0140-6736\(16\)30958-8](https://doi.org/10.1016/s0140-6736(16)30958-8) (2017).
- Gray, M. E. *et al.* Ovine pulmonary adenocarcinoma: A unique model to improve lung cancer research. *Front. Oncol.* **9**, 335. <https://doi.org/10.3389/fonc.2019.00335> (2019).
- Neal, R. D., Hamilton, W. & Rogers, T. K. Lung cancer. *BMJ* **349**, g6560. <https://doi.org/10.1136/bmj.g6560> (2014).
- Zhu, J., Wang, M. & Hu, D. Development of an autophagy-related gene prognostic signature in lung adenocarcinoma and lung squamous cell carcinoma. *PeerJ* **8**, e8288. <https://doi.org/10.7717/peerj.8288> (2020).
- Steven, A., Fisher, S. A. & Robinson, B. W. Immunotherapy for lung cancer. *Respirology* **21**, 821–833. <https://doi.org/10.1111/resp.12789> (2016).
- Hinshaw, D. C. & Shevde, L. A. The tumor microenvironment innately modulates cancer progression. *Cancer Res.* **79**, 4557–4566. <https://doi.org/10.1158/0008-5472.CAN-18-3962> (2019).
- Yang, L. V. Tumor microenvironment and metabolism. *Int. J. Mol. Sci.* **18**, 1–6. <https://doi.org/10.3390/ijms18122729> (2017).
- Arneth, B. Tumor microenvironment. *Medicina (Kaunas)* **56**, 1–21. <https://doi.org/10.3390/medicina56010015> (2019).
- Fridman, W. H., Pages, F., Sautes-Fridman, C. & Galon, J. The immune contexture in human tumours: Impact on clinical outcome. *Nat. Rev. Cancer* **12**, 298–306. <https://doi.org/10.1038/nrc3245> (2012).
- Hui, L. & Chen, Y. Tumor microenvironment: Sanctuary of the devil. *Cancer Lett.* **368**, 7–13. <https://doi.org/10.1016/j.canlet.2015.07.039> (2015).
- Kadara, F. *et al.* Whole-exome sequencing and immune profiling of early-stage lung adenocarcinoma with fully annotated clinical follow-up. *Ann. Oncol.* **28**, 75–82. <https://doi.org/10.1093/annonc/mdw436> (2017).
- Yang, Y. Cancer immunotherapy: Harnessing the immune system to battle cancer. *J. Clin. Invest.* **125**, 3335–3337. <https://doi.org/10.1172/JCI83871> (2015).
- Riley, R. S., June, C. H., Langer, R. & Mitchell, M. J. Delivery technologies for cancer immunotherapy. *Nat. Rev. Drug Discov.* **18**, 175–196. <https://doi.org/10.1038/s41573-018-0006-z> (2019).
- Topalian, S.L. *et al.* Safety, activity, and immune correlates of anti-PD-1 antibody in cancer. *N. Engl. J. Med.* **366**, 2443–2454. <https://doi.org/10.1056/NEJMoa1200690> (2012).
- Kennedy, L. B. & Salama, A. K. S. A review of cancer immunotherapy toxicity. *CA Cancer J. Clin.* **70**, 86–104. <https://doi.org/10.3322/caac.21596> (2020).
- Johnson, D. B., Jakubovic, B. D., Sibaud, V. & Sise, M. E. Balancing cancer immunotherapy efficacy and toxicity. *J. Allergy Clin. Immunol. Pract.* **8**, 2898–2906. <https://doi.org/10.1016/j.jaip.2020.06.028> (2020).
- Rashdan, S., Minna, J. D. & Gerber, D. E. Diagnosis and management of pulmonary toxicity associated with cancer immunotherapy. *Lancet Respir. Med.* **6**, 472–478. [https://doi.org/10.1016/s2213-2600\(18\)30172-3](https://doi.org/10.1016/s2213-2600(18)30172-3) (2018).
- Du, K., Zhang, L., Lee, T. & Sun, T. m(6)A RNA methylation controls neural development and is involved in human diseases. *Mol. Neurobiol.* **56**, 1596–1606. <https://doi.org/10.1007/s12035-018-1138-1> (2019).
- Wang, S. *et al.* Roles of RNA methylation by means of N(6)-methyladenosine (m(6)A) in human cancers. *Cancer Lett.* **408**, 112–120. <https://doi.org/10.1016/j.canlet.2017.08.030> (2017).
- He, L. *et al.* Functions of N⁶-methyladenosine and its role in cancer. *Mol. Cancer* **18**, 176. <https://doi.org/10.1186/s12943-019-1109-9> (2019).
- Sun, T., Wu, R. & Ming, L. The role of m⁶A RNA methylation in cancer. *Biomed. Pharmacother.* **112**, 108613. <https://doi.org/10.1016/j.biopha.2019.108613> (2019).
- Liu, Z. X., Li, L. M., Sun, H. L. & Liu, S. M. Link between m⁶A modification and cancers. *Front. Bioeng. Biotechnol.* **6**, 89. <https://doi.org/10.3389/fbioe.2018.00089> (2018).
- Shi, H., Wei, J. & He, C. Where, when, and how: Context-dependent functions of RNA methylation writers, readers, and erasers. *Mol. Cell* **74**, 640–650. <https://doi.org/10.1016/j.molcel.2019.04.025> (2019).
- Tong, J., Flavell, R. A. & Li, H. B. RNA m(6)A modification and its function in diseases. *Front. Med.* **12**, 481–489. <https://doi.org/10.1007/s11684-018-0654-8> (2018).
- Chen, X. Y., Zhang, J. & Zhu, J. S. The role of m(6)A RNA methylation in human cancer. *Mol. Cancer* **18**, 103. <https://doi.org/10.1186/s12943-019-1033-z> (2019).
- Yang, Y., Hsu, P. J., Chen, Y. S. & Yang, Y. G. Dynamic transcriptomic m(6)A decoration: Writers, erasers, readers and functions in RNA metabolism. *Cell Res.* **28**, 616–624. <https://doi.org/10.1038/s41422-018-0040-8> (2018).
- Zaccara, S., Ries, R. J. & Jaffrey, S. R. Reading, writing and erasing mRNA methylation. *Nat. Rev. Mol. Cell Biol.* **20**, 608–624. <https://doi.org/10.1038/s41580-019-0168-5> (2019).
- Wang, Q. *et al.* METTL3-mediated m⁶A modification of HDGF mRNA promotes gastric cancer progression and has prognostic significance. *Gut* **69**, 1193–1205. <https://doi.org/10.1136/gutjnl-2019-319639> (2020).
- Shi, Y. *et al.* YTHDF1 links hypoxia adaptation and non-small cell lung cancer progression. *Nat. Commun.* **10**, 4892. <https://doi.org/10.1038/s41467-019-12801-6> (2019).

32. Jin, D. *et al.* m(6)A demethylase ALKBH5 inhibits tumor growth and metastasis by reducing YTHDFs-mediated YAP expression and inhibiting miR-107/LATS2-mediated YAP activity in NSCLC. *Mol. Cancer* **19**, 40. <https://doi.org/10.1186/s12943-020-01161-1> (2020).
33. Li, N. *et al.* ALKBH5 regulates anti-PD-1 therapy response by modulating lactate and suppressive immune cell accumulation in tumor microenvironment. *Proc. Natl. Acad. Sci. USA* **117**, 20159–20170. <https://doi.org/10.1073/pnas.1918986117> (2020).
34. Wang, L. *et al.* m(6)A RNA methyltransferases METTL3/14 regulate immune responses to anti-PD-1 therapy. *EMBO J.* **39**, e104514. <https://doi.org/10.15252/embj.2020104514> (2020).
35. Kanehisa, M. & Goto, S. KEGG: Kyoto encyclopedia of genes and genomes. *Nucleic Acids Res.* **28**, 27–30. <https://doi.org/10.1093/nar/28.1.27> (2000).
36. Zhang, H. *et al.* Dynamic landscape and evolution of m⁶A methylation in human. *Nucleic Acids Res.* **48**, 6251–6264. <https://doi.org/10.1093/nar/gkaa347> (2020).
37. Reis, E. S., Mastellos, D. C., Ricklin, D., Mantovani, A. & Lambris, J. D. Complement in cancer: Untangling an intricate relationship. *Nat. Rev. Immunol.* **18**, 5–18. <https://doi.org/10.1038/nri.2017.97> (2018).
38. Han, B. *et al.* USP22 promotes development of lung adenocarcinoma through ubiquitination and immunosuppression. *Aging* **12**, 6990–7005. <https://doi.org/10.18632/aging.103056> (2020).
39. Zhang, X. M. *et al.* Prognostic and predictive values of immune infiltrate in patients with head and neck squamous cell carcinoma. *Hum. Pathol.* **82**, 104–112. <https://doi.org/10.1016/j.humpath.2018.07.012> (2018).
40. Li, X. *et al.* Identification of prognostic genes in adrenocortical carcinoma microenvironment based on bioinformatic methods. *Cancer Med.* **9**, 1161–1172. <https://doi.org/10.1002/cam4.2774> (2020).
41. Rosenthal, R. *et al.* Neoantigen-directed immune escape in lung cancer evolution. *Nature* **567**, 479–485. <https://doi.org/10.1038/s41586-019-1032-7> (2019).
42. Altorki, N. K. *et al.* The lung microenvironment: An important regulator of tumour growth and metastasis. *Nat. Rev. Cancer* **19**, 9–31. <https://doi.org/10.1038/s41568-018-0081-9> (2019).
43. Leonetti, A. *et al.* Molecular basis and rationale for combining immune checkpoint inhibitors with chemotherapy in non-small cell lung cancer. *Drug Resist. Updat.* **46**, 100644. <https://doi.org/10.1016/j.drug.2019.100644> (2019).
44. Desrichard, A., Snyder, A. & Chan, T. A. Cancer neoantigens and applications for immunotherapy. *Clin. Cancer Res.* **22**, 807–812. <https://doi.org/10.1158/1078-0432.CCR-14-3175> (2016).
45. Samstein, R. M. *et al.* Tumor mutational load predicts survival after immunotherapy across multiple cancer types. *Nat. Genet.* **51**, 202–206. <https://doi.org/10.1038/s41588-018-0312-8> (2019).
46. Zhang, L. *et al.* The prognostic value of TMB and the relationship between TMB and immune infiltration in head and neck squamous cell carcinoma: A gene expression-based study. *Oral Oncol.* **110**, 104943. <https://doi.org/10.1016/j.oraloncology.2020.104943> (2020).
47. Korman, A. J., Peggs, K. S. & Allison, J. P. Checkpoint blockade in cancer immunotherapy. *Adv. Immunol.* **90**, 297–339. [https://doi.org/10.1016/S0065-2776\(06\)90008-X](https://doi.org/10.1016/S0065-2776(06)90008-X) (2006).
48. Chen, R. *et al.* Targeting B7-1 in immunotherapy. *Med. Res. Rev.* **40**, 654–682. <https://doi.org/10.1002/med.21632> (2020).
49. Keler, T. *et al.* Activity and safety of CTLA-4 blockade combined with vaccines in cynomolgus macaques. *J. Immunol.* **171**, 6251–6259. <https://doi.org/10.4049/jimmunol.171.11.6251> (2003).
50. Zhang, B. *et al.* m(6)A regulator-mediated methylation modification patterns and tumor microenvironment infiltration characterization in gastric cancer. *Mol. Cancer* **19**, 53. <https://doi.org/10.1186/s12943-020-01170-0> (2020).
51. Zhong, J. *et al.* m(6)A modification patterns and tumor immune landscape in clear cell renal carcinoma. *J. Immunother. Cancer* **9**, 1–12. <https://doi.org/10.1136/jitc-2020-001646> (2021).

Acknowledgements

The authors would like to thank 51runse, Toweree (Beijing) Education Company, for editing the manuscript.

Author contributions

Z.B. performed study concept, design, review and revision of the paper; X.W. performed development of methodology and writing, acquisition, analysis and interpretation of data, statistical analysis, and technical and material support. All authors read and approved the final paper.

Competing interests

The authors declare no competing interests.

Additional information

Supplementary Information The online version contains supplementary material available at <https://doi.org/10.1038/s41598-021-00272-z>.

Correspondence and requests for materials should be addressed to Z.B.

Reprints and permissions information is available at www.nature.com/reprints.

Publisher's note Springer Nature remains neutral with regard to jurisdictional claims in published maps and institutional affiliations.



Open Access This article is licensed under a Creative Commons Attribution 4.0 International License, which permits use, sharing, adaptation, distribution and reproduction in any medium or format, as long as you give appropriate credit to the original author(s) and the source, provide a link to the Creative Commons licence, and indicate if changes were made. The images or other third party material in this article are included in the article's Creative Commons licence, unless indicated otherwise in a credit line to the material. If material is not included in the article's Creative Commons licence and your intended use is not permitted by statutory regulation or exceeds the permitted use, you will need to obtain permission directly from the copyright holder. To view a copy of this licence, visit <http://creativecommons.org/licenses/by/4.0/>.

© The Author(s) 2021